The 8th European Congress on Computational Methods in Applied Sciences and Engineering
ECCOMAS Congress 2022
5 – 9 June 2022, Oslo, Norway

LATTICE BOLTZMANN SIMULATION OF A DEPLOYING KRUEGER DEVICE

JORGE PONSIN[*] AND CARLOS LOZANO[†]

Computational Aerodynamics Group
National Institute of Aerospace Technology (INTA).
Carretera de Ajalvir, km 4. Torrejón de Ardoz 28850, Spain
[*]e-mail: ponsinj@inta.es, [†] lozanorc@inta.es. http://uhura-project.eu

Key words: Lattice Boltzmann.

Summary. In this paper, we describe the numerical simulations carried out within the H2020 UHURA project of the turbulent unsteady flow generated during the motion of a Krueger device for laminar wings using a commercial lattice Boltzmann solver based on a Wall-Modelled LES approach. The simulations are focused on reproducing one of the experimental test cases carried out in the ONERA-L1 wind tunnel during the UHURA project. The numerical method and the simulation setup are described. The simulation results are compared with the high-quality experimental data obtained in the ONERA-L1 wind tunnel in order to assess the accuracy of the predictions.

1 INTRODUCTION

Laminar flow wing technology is a promising avenue that can lead to a significant reduction in drag and consequent fuel consumption. It requires specific high-lift concepts that are subject to the main constraint that in cruise conditions, and with the device in retracted position, the flow on the upper surface must remain unperturbed. One possible solution is to replace the classical slat element with a folded Krueger device [1]. The unsteady flow present during the fast deployment and retraction of a Krueger device is quite complex, with massive turbulent flow separation in some phases of the motion, and strong dynamical effects are expected. Therefore, the unsteady CFD flow prediction is a big challenge requiring improved standard tools based on URANS solvers complemented by high-fidelity CFD tools based on scale-resolving simulation methods. Furthermore, detailed experimental data is required to validate the CFD predictions and to understand the flow physics produced by the motion of the Krueger.

The EU funded UHURA project aims chiefly at performing experimental research on the unsteady complex flow behaviour associated to the deployment/retraction of a Krueger device mounted on a laminar wing. Additionally, it seeks to improve and validate unsteady CFD simulation methodologies. The focus is set on URANS solvers and the special grid techniques required to dealing with large element motions (chimera, immersed boundaries, etc). Additionally, other unsteady flow methodologies are investigated, such as advanced hybrid RAN-LES turbulence models as well as alternative CFD techniques such as the Lattice Boltzmann Method (LBM).

This paper presents a nearly completed study of the application of the LBM methodology to the prediction of the unsteady flow around a deploying/retracting Krueger device carried out by INTA within the UHURA project. Our aim is twofold: to assess and validate LBM on these type of flows and, second, to complement the URANS computations performed by the majority of partners with scale-resolving simulations.

2 SIMULATION METHODOLOGY

2.1 Lattice-Boltzmann methods

The LBM is a promising alternative method for the simulation of unsteady flows due to several reasons: first, it is intrinsically unsteady and has very low numerical dissipation/dispersion errors, which makes it suitable for joint use with high-fidelity turbulence models based on scale resolving methodologies. Second, its underlying adaptive Cartesian octree mesh approach, together with the way wall boundary conditions are imposed, is particularly well suited to dealing with complex and/or moving geometries. Finally, the approach is computationally extremely efficient (even though the time step advancement is limited by the explicit stepping nature of the time integration method). The LBM is a mesoscopic CFD approach that is based on numerically solving a discretized version of the Boltzmann transport equation for the probability distribution function of particles at a given spatial location and velocity. Macroscopic flow properties such as density, velocity and pressure, arise as the successive (velocity) moments of the distribution functions. It can be shown theoretically that the isothermal weakly compressible NS equations are recovered from a Chapman-Enskog (multiscale) expansion of the moments of the LBM equations.

2.2 Computational methodology

Scheme

Within the UHURA Project, INTA is using the commercial LBM code Simulia-*XFlow* [2]. *XFlow* is based on a three dimensional 27-velocity lattice model (D3Q27), which seems to be the most appropriate set of velocities for turbulent computations due to the higher level of symmetry of the velocity lattice. The collision operator is based on a *central moment* model that has a high degree of accuracy and stability, and benefits from an extended Mach number application range compared to standard collision operators.

Turbulence modelling

XFlow uses a LES approach with the wall-adapting local eddy viscosity (WALE) SGS model. This is supplemented with a wall shear-stress based wall-modelled LES (WMLES) approach with a non-equilibrium algebraic wall function.

Meshing

The meshing approach is based on an adaptive Octree Cartesian technique, where the number and arrangement of Octree levels depends on the far-field and minimum resolutions specified in the geometry as well as the prescribed buffer layers among different levels. On-the-fly adaptive mesh refinement is used in dynamic motions. The mesh is adapted in the near wall region to guarantee sufficient resolution for the wall turbulence model. In addition, a

dynamic adaptive algorithm based on the local level of vorticity has been used to resolve the wakes and large separation areas. These two adaptive options are only available for parallel shared-memory architectures in the used version of the code, which limits the mesh sizes that can be used in the simulations.

Dynamic motion

Dynamic motion is handled with an immersed moving boundary method based on a modified partially saturated cell method (PSM) which amounts, roughly speaking, to a modification of the collision operators with an additional term proportional to the solid volume fraction of the cell. This algorithm has (roughly) a 40% CPU time overhead with respect to static computations (fixed geometry).

3 STAGE 1: NUMERICAL SETUP

During the first part of the UHURA project (WP2), research activities were dedicated to studying the sensitivity of the computations to grid resolution and numerical setup, in order to perform accurate static/dynamic WMLES simulations of the Krueger flap with reasonable CPU time cost. Here, we give a brief overview of the work performed in this stage. A thorough account of these activities can be found in [3][4]. The investigations where mainly focused on the following items:

1) Establish the minimum boundary layer resolution for LBM-WMLES
2) Find the appropriate mesh resolution for high curvature regions (i.e., near the main element's leading edge)
3) Find the appropriate mesh resolution for adequately resolving large scales in wakes
4) Fix the appropriate spanwise domain extension L_z, as an extruded 2.5D approach will be used.
5) Find the appropriate time steps, simulation times for statistics (static cases), averaging time, etc.

Two main lessons were extracted from these preliminary analyses. The first one is that the deploying Krueger test case is very challenging for LBM and, thus, it requires a careful numerical set up and mesh design, paying special attention to mesh resolution in certain areas.

The second lesson is that XFlow's shear-stress-based WMLES approach has difficulties to properly model the physics close to the wall. It was observed that transition to turbulence is not always produced on boundary layers (especially at the upper main wing), leading to under resolved turbulent boundary layers (Figure 1). In fact, turbulence is present on the upper side of the main wing only in some phases of the deployment/retraction, when it is triggered by strong incoming flow perturbations. In any other case, lack of turbulent content results in the under-prediction of turbulent boundary layer (TBL) effects along the upper main wing, and also affects shear layers downstream of the main element, resulting, overall, in an over-prediction of lift compared to RANS simulations.

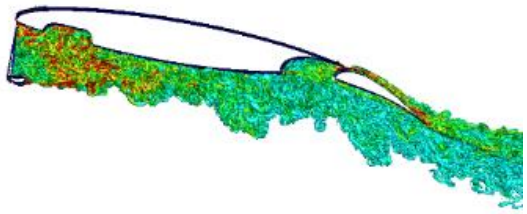

Figure 1. Iso-surface of Q parameter coloured by vorticity for the Krueger device in perpendicular position.

This type of problem is not unheard of in general WMLES models (not necessarily LBM), and different strategies have been devised to trigger turbulent fluctuations in modelled boundary layers. In our case, an exploratory study on tripping transition using cylindrical roughness elements [5] was carried out (Figure 2). The elements produce a rapid switch to turbulence of the boundary layer, resulting in improved cp and lift predictions at the cost of increased computational cost and undesirable influence on the flow upstream of their location, so they were not used in the validation phase of the project (WP4).

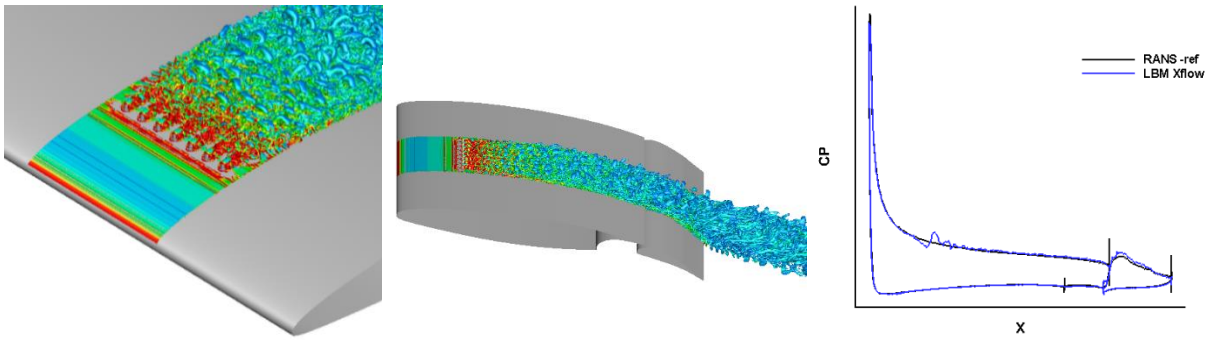

Figure 2. Iso-surface of Q parameter coloured by vorticity and Cp distribution for the Krueger device in retracted position with roughness elements.

4 STAGE 2: ASSESMENT AND VALIDATION

The second stage of the project (WP4) corresponds to the validation of the final geometry against experimental data. Due to computational and time constraints, we have focused in reproducing the conditions of the ONERA L1 wind tunnel campaign [6]. Overall, one dynamic and 10 static computations have been carried out. The dynamic computation simulates a complete deployment/retraction cycle at velocity U = 30 m/s with deployment/retraction and holding times 1 s and 0.25 s, respectively, for a total of 2.25 s. The motion of the Krueger device has been obtained from experimental measurements of the isolated drive engine [7]. Static computations, on the other hand, have been performed for five fixed positions of the Krueger device at two velocities U = 30 m/s and U = 45 m/s. Static computations are used to assess the influence of the Reynolds number on the results and, additionally, to assess the influence of dynamic effects by comparing the static cases at U = 30m/s to the dynamic simulation. A thorough account of these activities can be found in [8].

4.1 Computational set-up

The geometry used in the simulations corresponds to the DLR- F15 configuration modified with a laminar leading-edge Krueger device immersed in a simplified rendition of the ONERA L1 tunnel. The CAD model of the wing and the ONERA-L1 wind tunnel section were provided by DLR [9]. High resolution STL surface meshes were generated from these geometries using an in-house tool. With the available computational resources, it is not possible to simulate the complete wind tunnel test section with LBM-WMLES. Therefore, as shown in Figure 3, the computational domain has been designed to reproduce the effect of the ONERA-L1 wind tunnel section walls in a simplified manner. The upper and lower walls have been placed at their real location relative to the model, and have been prescribed as slip walls. The longitudinal size of the WT has been enlarged up to 4 times the original WT section length in order to decrease the impact of the inlet and outlet boundary conditions on the flow at the location of the configuration. The span-wise size, L_z, is set to 0.24 m, which is about twice the length of the Krueger panel and $1/10^{th}$ of the width of the ONERA L1 wind tunnel. This should be large enough to contain the largest (3D) turbulent structures produced in the wake area behind the Krueger device. Notice that, with this settings, our simulations do not distinguish between the part-span or full-span models tested in the ONERA-L1 W/T.

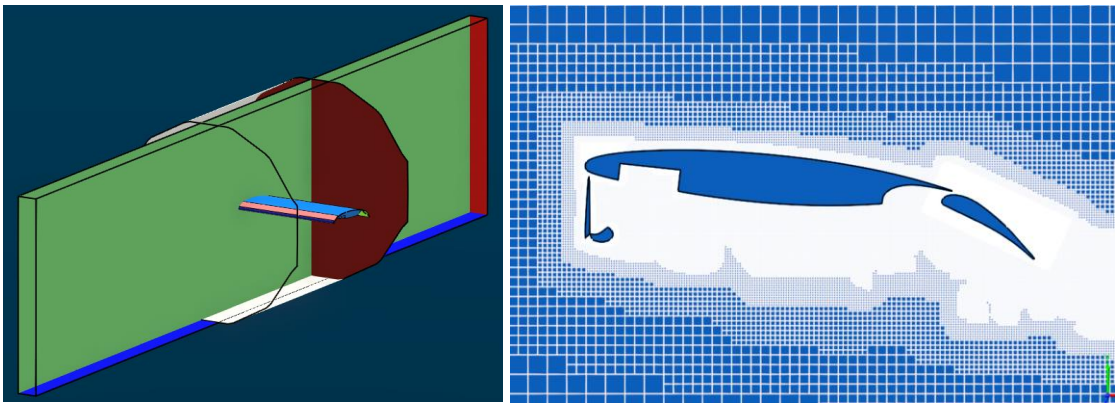

Figure 3. Left: Schematics of the computational domain. The ONERA-L1 wind tunnel section (maroon octagonal shape) is also shown for reference. Right: Snapshot of the instantaneous computational mesh.

4.2 Meshing details

Mesh resolutions are carefully designed in each area to capture the relevant structures. On the main wing, the minimum resolution $\Delta_{\min}$ is set to $\Delta_{\min} / C_{ref} \sim 2\times10^{-3}$ where C_{ref} is the length of the wing in retracted position, resulting in roughly 10 cells within the boundary layer. The resolution is doubled at the leading edge of the wing and at the rear flap area, while it is set to $\Delta_{\min} / C_{ref} \sim 6.25\times10^{-4}$ at the Krueger device. Dynamic mesh adaptation with a target resolution $\Delta_{\min} / C_{ref} \sim 2.25\times10^{-3}$ is prescribed at the wake behind the Krueger device. Overall, these choices result in mesh sizes ranging from 12 M cells for the retracted position up to 16 M cells for the Krueger at 75º.

4.3 Numerical settings

- **Boundary conditions:** An inlet velocity has been prescribed at the inlet of the domain, while characteristic outflow non-reflecting boundary conditions have been applied at the outlet. Periodicity has been used for the side walls, and slip boundary conditions have been used for the upper and lower walls of the domain. No synthetic turbulence is imposed at any station and no roughness elements have been used to trip turbulence.
- **Time step and Mach number influence:** The time step of the simulations is given in terms of the Mach number and spatial resolution by an acoustic scaling as $\Delta t = (1/\sqrt{3})\Delta x M / U_\infty$. Choosing Mach numbers M = 0.1 for U_∞ = 30 m/s and M = 0.15 for U_∞ = 45 m/s yields time steps at the finest grid levels $\Delta t_{\min} U_\infty / C_{ref} = 4.5\times10^{-5}$ and $\Delta t_{\min} U_\infty / C_{ref} = 6.75\times10^{-5}$, respectively.
- **Running strategy and collection of statistics:** Static simulations were run for about 15-25 convective time units (CTU), depending on the test case, after which averaged statistics (mean values of global quantities of interest and pressure distributions) were collected for about 5-10 additional CTU's.

5 RESULTS

Figure 4 shows a breakdown by components of the lift history for a dynamical simulation spanning a full deployment-retraction cycle (1s deployment time, 0.25s holding time, 1s retraction time). Conditions are aoa = 6º, U = 30m/s and Re = 1.23 Mill. We note that there is a significant loss of total lift that comes basically from the rear flap and the main wing.

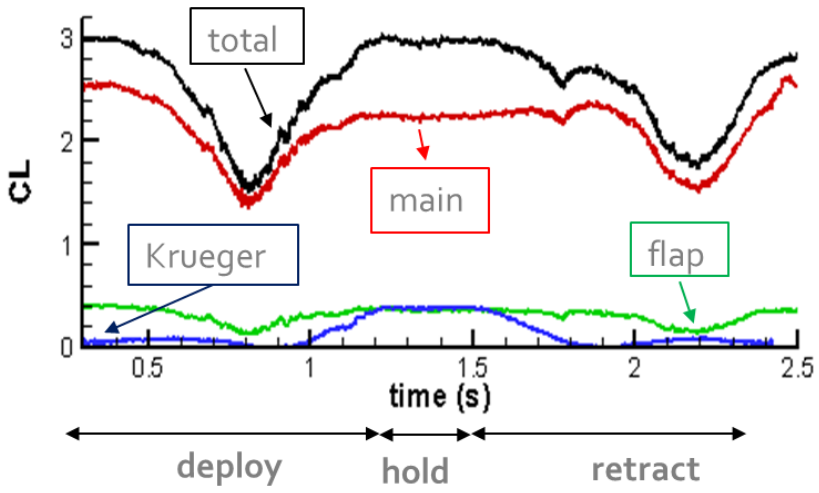

Figure 4. Lift history for a full deployment/retraction cycle. Deployment starts at t = 0.25 s.

This loss of lift occurs at different positions of the Krueger panel in the deployment and retraction phases. This is a significant dynamical effect (hysteresis) caused by the stall of the rear flap at different deflections of the Krueger device during motion (Figure 5 & Figure 6). The hysteresis is not observed on the Krueger device itself (Figure 6, right), in agreement with ONERA [10] and DNW-NWB [11] experimental results.

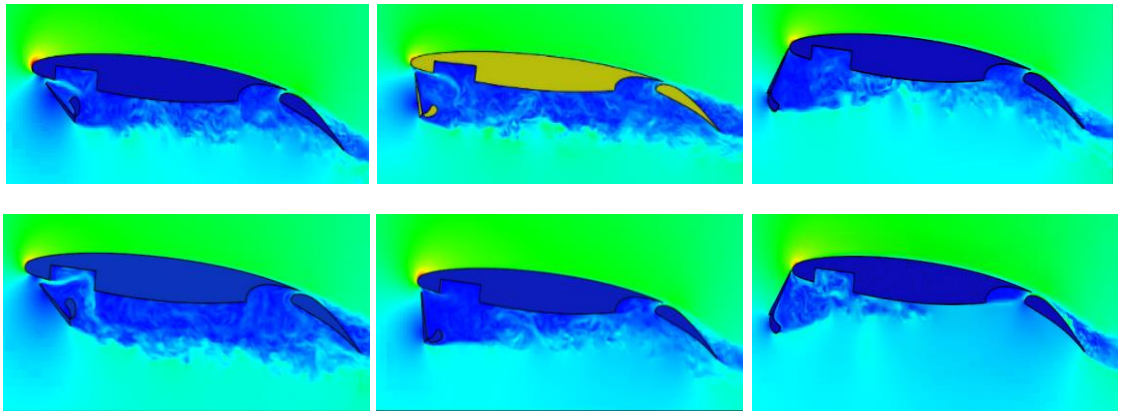

Figure 5. Snapshots of the instantaneous velocity field during a complete cycle. Upper row: deployment phase, left to right (37.5º, 75º, 112.5º). Lower row: retraction phase, right to left (112.5º, 75º, 37.5º). Lift minima occur at 75º during deployment and 37.5º during retraction.

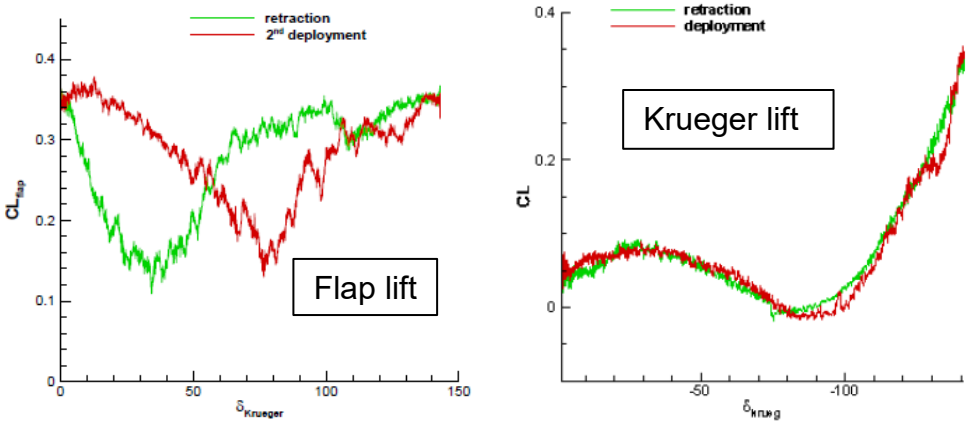

Figure 6. Evolution of lift and drag with respect to the Krueger panel deflection angle for the rear flap (left) and the Krueger panel (right).

Static simulations at U = 30 m/s are quite similar to dynamic simulations during the deployment phase (Figure 7), except at $\delta_{Krueger}$ = 37.5º, where the static simulations predict a reduced lift on the flap and main elements. The opposite occurs for the retraction phase. In this case, a large discrepancy occurs at $\delta_{Krueger}$ = 75º, when the Krueger is in nearly-perpendicular position relative to the wing. The static simulations predict the maximum loss of lift, while for the retracting dynamic simulation this is delayed until the Krueger panel reaches an angle close to 37.5º. This is further explored in Figure 8, which compares the instantaneous flow fields at $\delta_{Krueger}$ = 75º illustrating the differences between the predicted wake properties in dynamic and static simulations. Notice also that there are only small differences between the static results at 30m/s and 45m/s, in agreement with ONERA L1 W/T results (Figure 9).

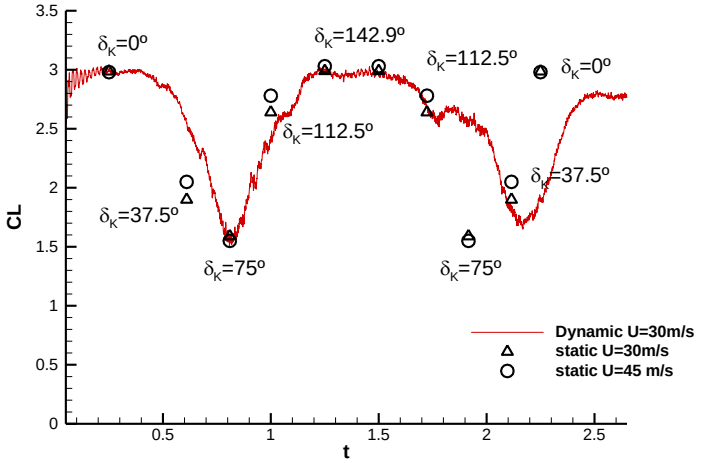

Figure 7. Comparison of predicted lift for dynamic (U=30m/s, red) and static time-averaged computations (Re=1.23 Mill vs Re=1.85 Mill)

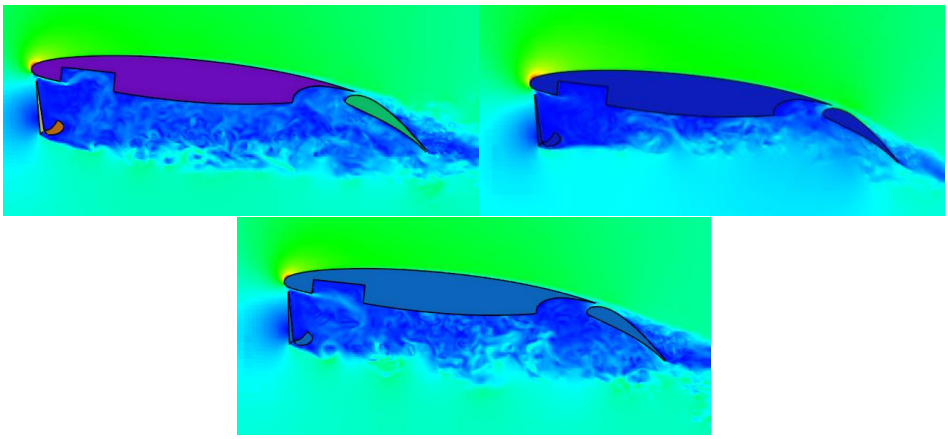

Figure 8. Instantaneous flow velocity at $\delta_{Krueger}$ = 75º for dynamic deployment (top left), dynamic retraction (top right) and static (bottom) cases.

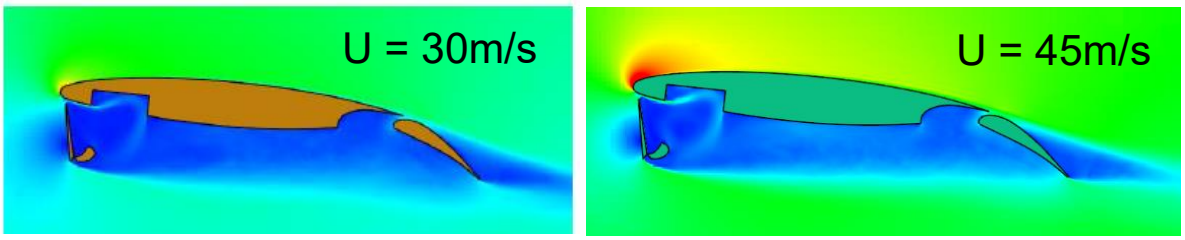

Figure 9. Averaged flow fields at $\delta_{Krueger}$ = 75º for static computations at U = 30 m/s and U = 45 m/s.

Figure 10 and Figure 11 compare the numerical and experimental pressure distributions at 5 positions of the Krueger device in the low-velocity case U = 30m/s for the deployment and retraction phases. The figures show instantaneous data from dynamic simulations, time-averaged data from static simulations and phase-averaged MEMS located on the wing leading edge and Krueger panel (as indicated in Figure 10). We see that the predicted Cps are in reasonable agreement with experiments. In the deployment phase, there is an over-prediction of suction for all angles, and the minimum wing lift, in which the flap is stalled, is observed in

simulations close to 75º. In the retraction phase, on the other hand, the minimum wing lift is observed in dynamic simulations close to 37.5º, with the flap again stalled.

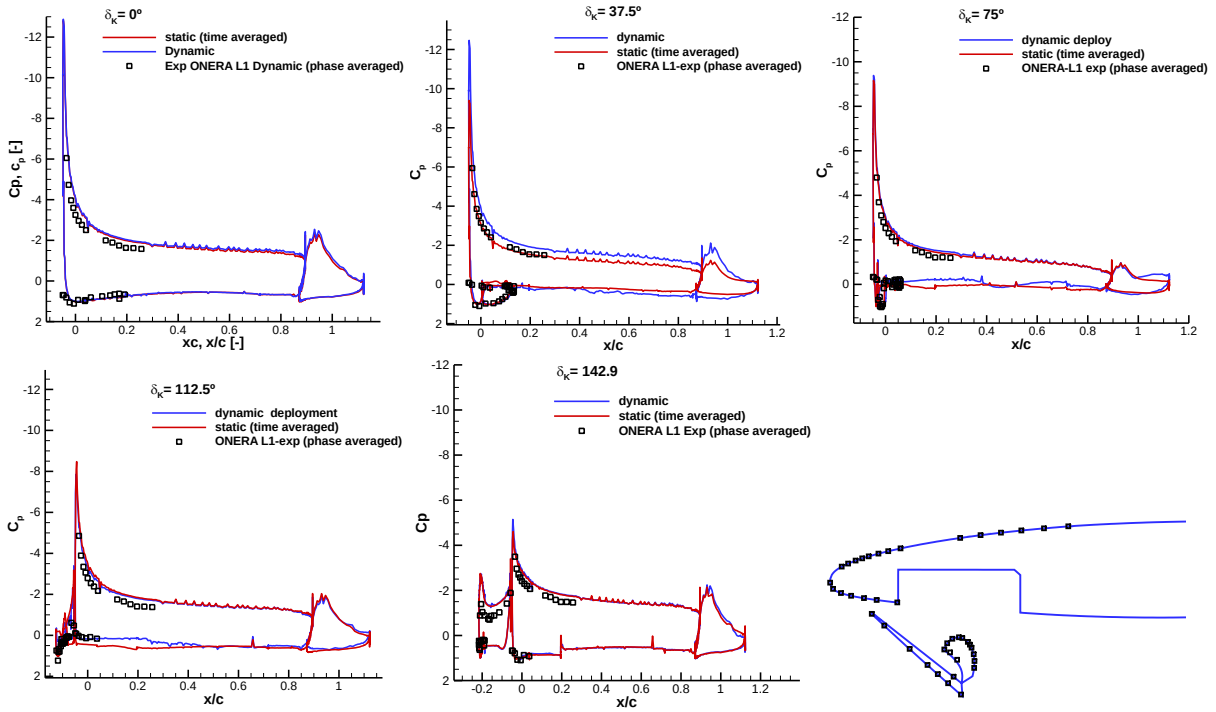

Figure 10. Numerical (static & dynamic) vs. experimental pressure distributions (ONERA L1) during deployment.

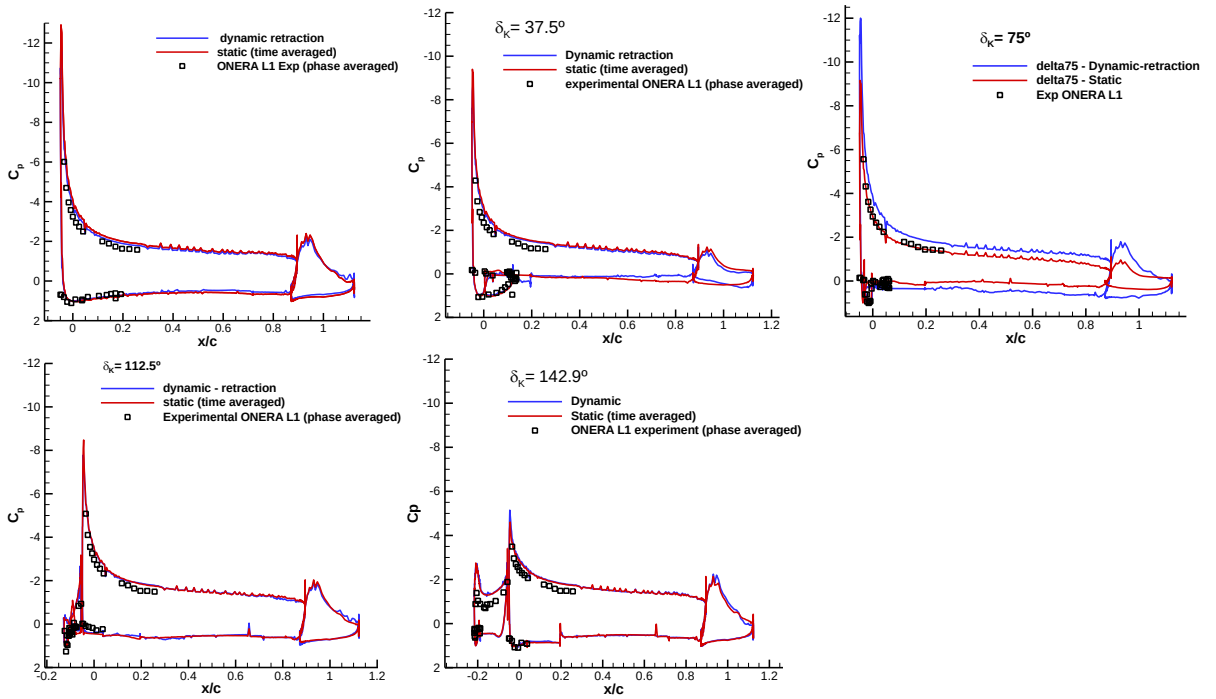

Figure 11. Numerical (static & dynamic) vs. experimental pressure distributions (ONERA L1) during retraction.

Figure 12 compares experimental and simulated lift in regard to dynamical effects. The

experimental value for lift is obtained by integrating the main wing leading edge Cps (MEMS), and is used as a proxy for the total wing lift history during deployment/retraction, while simulation data corresponds to the total main wing lift. Notice that experimental results confirm the hysteresis effect between deployment and retraction, which is however not observed in the DNW-NWB experiment at the same flow conditions. Both results agree in the prediction of Krueger panel deflections for minimum lift at deployment/retraction phases, with a + 5º delay between simulation and experiment, and the behavior of the retraction phase is qualitatively well reproduced by the simulations.

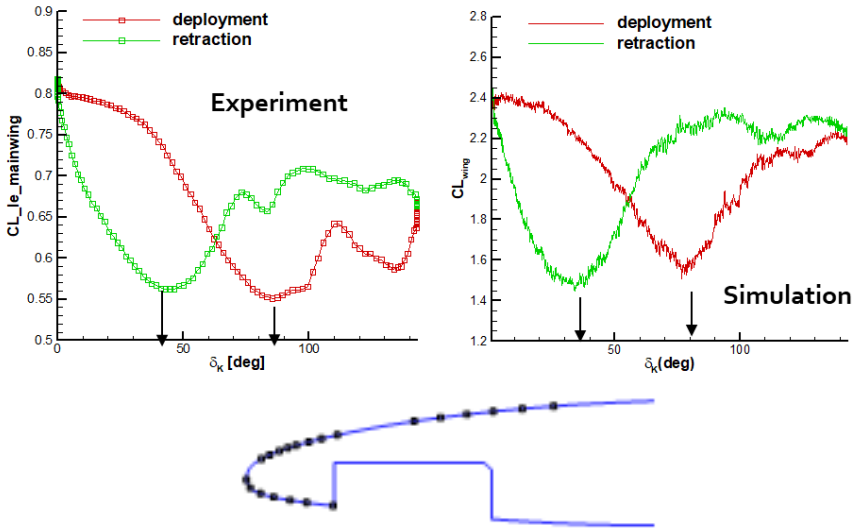

Figure 12. Computed lift vs. experimental lift for the front section of the main wing.

Finally, Figure 13 and Figure 14 compare time-averaged numerical results with PIV data from the ONERA L1 wind tunnel at several static positions of the Krueger device for the high-velocity case (U = 45m/s). Qualitatively, there is a fair agreement of the numerical results with PIV experiments, particularly in the prediction of zones of reverse flow and of the areas with high turbulent kinetic energy.

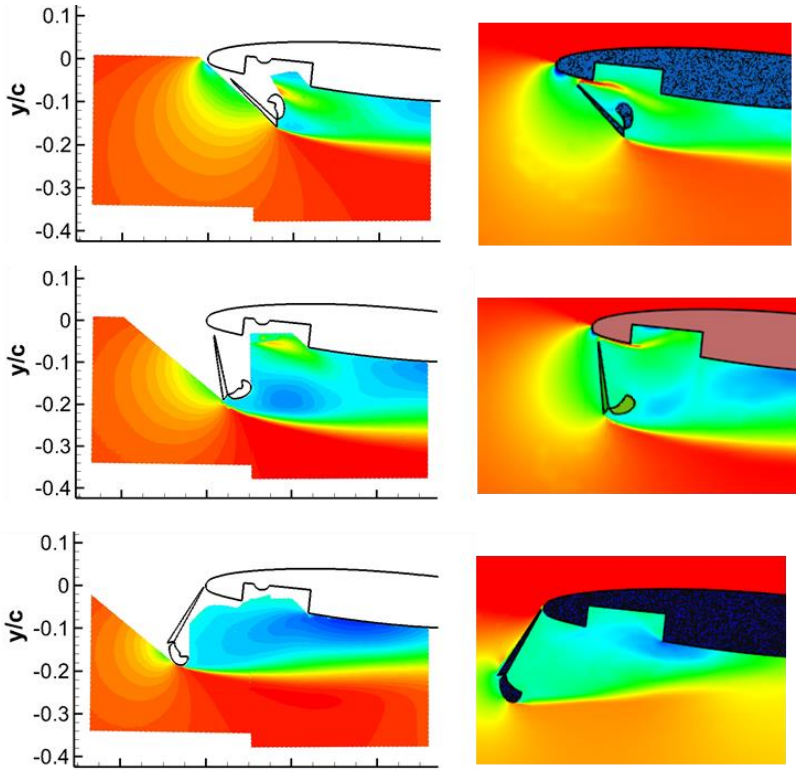

Figure 13. Averaged velocity flow. Left: PIV ONERA L1 results. Right: LBM results

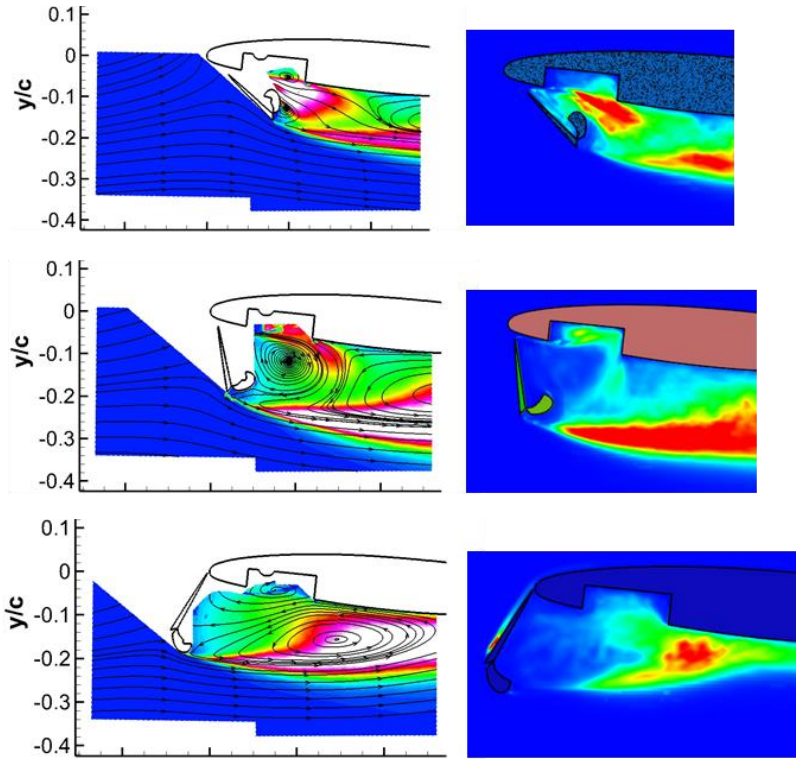

Figure 14. Averaged turbulent kinetic energy. Left: PIV ONERA L1 results. Right: LBM results (resolved tke).

6 CONCLUSIONS

- Lattice Boltzmann methods show great potential for robust and efficient simulation of deploying high lift geometries.
- The deploying Krueger case has proven very challenging for the used LBM approach due to accuracy limitations of the methodology used near walls (WMLES + Cartesian mesh).
- Despite the problems found with the near-wall turbulence-modelling approach, pressure distributions and forces are in reasonable agreement with experimental data.
- Strong dynamical effects are predicted for the ONERA L1 full span configuration.
- Averaged flow field compares well with ONERA's PIV results.
- Validation activities and comparison with other CFD's still ongoing.

ACKNOWLEDGEMENTS

The project leading to this publication has received funding from the European Union's Horizon 2020 Research and Innovation Programme under grant agreement Nº 769088.

REFERENCES

[1] Iannelli P., Wild J. et al. Analysis and applications of suitable CFD–based optimization strategies for high-lift system design. ECCOMAS 2012 Proceedings, paper 2833.
[2] Trapani G., Brionnaud R. and Holman D. XFlow contribution to the third High-Lift prediction workshop AIAA 2018-2847, 2018 AIAA Applied Aerodynamics Conference.
[3] Ponsin J. and Lozano C. Technical report on assessment of LBM and best practices for the prediction on unsteady aerodynamics during deployment/retraction phases of high lift systems. UHURA Deliverable D22-2, 2020.
[4] Ponsin J. and Lozano C. Progress towards simulation of Krueger device motion with Lattice Boltzmann Methods. IOP Conf. Ser.: Mater. Sci. Eng. 1024 (2021) 012050.
[5] Deck S., Weiss P. and Renard N. J. Comput. Physics 363 (2018), 231-255
[6] Tanguy G. Test Matrix for ONERA L1 Wind Tunnel test. UHURA Deliverable D33-1.
[7] UHURA Coordination Memorandum nº UH-31-CM16: Krueger deflection time data
[8] Ponsin J. and Lozano C. Summary of lattice Boltzmann LES technique results for aero-loads prediction. UHURA Deliverable D41-5, 2022.
[9] UHURA Coordination Memorandum nº UH-31-CM12: Final shape of DLR-F15-LLE Krueger flap for wind tunnel testing.
[10] Tanguy G. Data of ONERA L1 wind tunnel test. UHURA Deliverable D33-3, 2022.
[11] UHURA Coordination Memorandum nº UH-42-CM22: Averaged data from DNW tests.